Creep Behaviour of Inconel 718 Processed by laser powder bed fusion

Zhengkai Xu, C. J. Hyde, C. Tuck & A. T. Clare

Department of Mechanical, Materials and Manufacturing Engineering, University of Nottingham, University Park, NG7 2RD, United Kingdom

Abstract

Additive manufacturing lends itself well to the manufacture of aerospace parts due to the high complexity and small volume of many components found in modern aero engines. By exploiting additive manufacturing design freedoms, enhanced part functionality can be achieved and lead time can be reduced. However, the integrity of these parts is a primary concern which often cannot be guaranteed with current generation additive manufacturing methods and materials. Studies on the performance of additively manufactured parts under service conditions are therefore required.

In this study, laser powder bed fusion is used to produce specimens for creep testing. To allow this a novel specimen design, i.e. Two Bar Specimen, was applied for creep testing. The performance of these specimens, in the as-build condition, is showed to be largely poor because of surface integrity defects, in-built pores, and unfavourable microstructure formation. These are clearly highlighted and explored. Further specimens, subjected to heat treatments, have also been tested. These showed a marked improvement of the microstructure and hence creep performance. The lifetime of heat-treated samples was enhanced by as much as four times compared to the as-build specimens. However, this lifetime performance remains 33 percent below that of samples machined from the equivalent wrought material. This work then proposes manufacturing strategies to significantly enhance the performance of Inconel 718 when processed via laser powder bed fusion and post-heat-treatments.

Keywords: *Creep, Two Bar Specimen, Additive Manufacture, Inconel 718, Laser powder bed fusion*

1. Introduction

Laser powder bed fusion (LPBF) selectively melts the powder bed according to a 3D CAD model with a focused laser beam and builds components layer by layer (Gibson et al., 2010). Since LPBF is a

process that can produce dense metal components directly from CAD data without the need for tooling, it offers great advantages for fabricating complex components, such as those made from superalloys for aerospace applications (Wang, 2011). However, the high-temperature performance of LPBF components, in terms of, microstructures and mechanical properties compared to traditionally manufactured equivalent has not been fully studied (Song et al., 2015).

Inconel 718 is one of the most popular materials applied in modern aero engines (Schafrik et al., 2001). Multiple strengthening mechanisms, such as precipitation hardening and solid solution hardening, make it possible for Inconel 718 superalloy to retain high strength and fatigue resistance at elevated temperatures as high as 650°C (Diltemiz and Zhang, 2013). But, the mechanical properties sought for such engineering application inevitably leads to poor machinability. Special tools and carefully selected machining parameters are required (Qi et al., 2009). However, in the LPBF process, a material's "machinability" is no longer an issue. In the LPBF manufactured components, the microstructure is normally columnar dendrites which grow epitaxially along the building direction (Liu et al., 2011). LPBF of Inconel 718 has also been investigated by Amato et al. (2012) who studied the microstructure and basic mechanical properties, such as hardness and tensile properties, of LPBF fabricated Inconel 718 structures. However, the high temperature creep performance of LPBF made Inconel 718 specimens, has not been evaluated. Processing parameters were found have influences on LPBF manufactured components. Lu et al. (2015) demonstrated that different island scanning strategies can lead to different relatively density, ductility and residual stress. Both Xia et al. (2016) and Nadammal et al. (2017) studied the effects of hatch spacing. Xia et al. (2016) modelled the mass and heat transfer in the molten pool, found hatch spacing played a critical role in determining structures' surface quality. A hatch spacing of 60 μm was applied in their study and result an average surface roughness of 2.23 μm. Nadammal et al. (2017) noticed ten times increase of the hatch spacing can lead to a texture intensity decrease by a factor of two. They also concluded that the thermal gradients influenced by the hatch spacing is one of the main factors that lead to the residual stress variation. Yadollahi et al. (2017) investigated the effects of building direction on the fatigue performance of LPBF manufactured components. Specimens possess the highest fatigue strength when building direction perpendicular to the loading direction. Since defects between layers are more detrimental when loading direction and building direction are the same. The reuse of the metal

powder is a big issue in the LPBF process. Hann (2016) proved the reuse of powder in LPBF of Inconel 718 can slightly increase oxygen content in powders but has little influence on the mechanical properties. As regard to the post processing of LPBF manufactured components, Heat treatment (HT) and Hot Isostatic Pressing (HIP) are the most commonly used techniques. The effects of stress relief (SR) heat treatment, HT and HIP were studied by Prater et al. (2015). SR specimens possess the worst ultimate tensile stress and yield stress. As built and SR+HIP specimens possess similar ultimate tensile stress and yield stress. Specimens treated with SR+HIP+HT are the best. Tucho et al. (2017) carefully analysed the microstructure and hardness of as-machined and solution heat treated Inconel 718 specimens. Laves phases are the main precipitates on the grain boundaries and sub-grain boundaries of as-machined specimens. While after solution heat treatment, (Nb,Ti)C carbides become more commonly seen, and the hardness become smaller after heat treatment. Due to the fast heating and cooling process in the LPBF, residual stress is an important issue which will has effects on components' quality and their mechanical properties. As mentioned by Mercelis and Kruth (2006), residual stress generated in the LPBF process are controlled by a variety of aspects such as the building height of samples. Higher building height can lead to higher positive residual stress to the top layer of the samples. While the base plate removal with Wire EDM can release the residual stress.

Creep resistance is one of the major life-limiting properties for high-temperature components in aero engines. It is affected by both working environment and the microstructure of the components (Diboine and Pineau, 1987). According to Kassner (2009), the nucleation of cavities in commercial alloys are usually observed on grain boundaries and associated with the existence of second-phase particles. Grain-boundary sliding and dislocation pile-ups are two of the main mechanisms that control the nucleation of cavities. Liu et al. (1991) demonstrated that grain size and carbide structure strongly influence creep crack growth in Inconel 718. The function of these carbide precipitates is twofold, for example, δ phase, as discussed by Parimi et al. (2014), can improve creep resistance, while some other types of precipitates (e.g. Laves phase) are detrimental. Based on the mechanism of creep (Ashby and Jones, 2012), large grain sizes and strengthening precipitates, such as δ phase, on grain boundaries are preferred in order to improve creep resistance.

Surface integrity is a key issue that needs to be considered in specimen preparation. Surface integrity includes many aspects such as basic surface finish, macro-structures, microstructures and even more complicated data sets such as residual stress conditions and other mechanical defects (M'Saoubi et al., 2008). In the study made by Wen et al. (2016), surface roughness was found to have some effect upon creep performance in a stress range smaller than 150MPa. Their analytical results also showed that the effects of surface roughness on damage will decrease when the stress is higher than 150MPa. This was because the surface of the sample tends to get flattened under high stress. However, there are few studies with respect to the effects of other surface finish conditions on creep performance. Many studies have also reported the detrimental effects of "white layers" on fatigue resistance, however, no studies considered white layers effects on creep resistance.

Here, the creep behaviour of LPBF manufactured Inconel 718 specimens is evaluated by using a newly developed two-bar specimen (TBS) creep testing method (Hyde et al., 2013). The main mechanisms that lead to specimen failure and the effects of heat treatments on the creep resistance of LPBF built specimens is explored. It is also made clear in this study that the surface integrity of LPBF produced components is critical in determining the creep performance of these specimens. This serves to identify key consideration for manufacturing chains which make use of laser-based additive manufacture. As part of a wider study, the effects of LPBF building direction and the role of residual stress in the creep testing are not considered in this paper.

2. Methodology and Materials

Creep testing using two bar specimens (TBS) was undertaken by Hyde et al. (2013) and Ali et al. (2015) to investigate the creep behaviour of Grade P91 steel at 650˚C. This test arrangement allows for scaled and relatively rapid creep testing. The results obtained agreed with those obtained in standard uniaxial specimen creep testing. The dimensions of the two bar specimens applied in this study are showed in Figure 1.
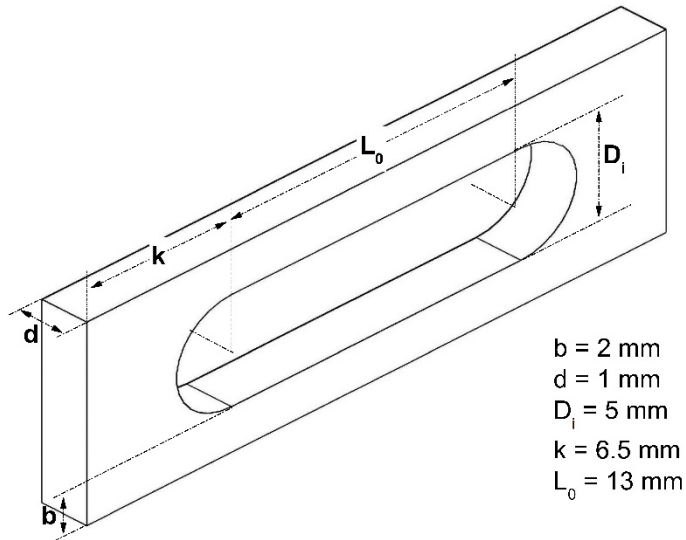
b = 2 mm
d = 1 mm
D_i = 5 mm
k = 6.5 mm
L_0 = 13 mm

Figure 1 Schematic of two bar specimen and its dimensions

Equation 1 has been used to convert the stress applied to the TBS creep testing into a corresponding equivalent uniaxial stress so that the data obtained in two bar specimen creep testing can be compared with those obtained in standard uniaxial specimen creep testing. This method was discussed in the study made by Ali et al. (2015).

$$\sigma_{ref} = \eta \sigma_{nom}$$

Equation 1 (Ali et al., 2015)

Where σ_{ref} is the stress applied in two bar specimen and σ_{nom} is the nominal stress applied in the corresponding standard uniaxial specimen. η is a constant which relates to the geometry of specimen and for which the calculation method and value ($\eta = 0.9966$) for the geometry applied in this study can be found in the study made by Hyde et al. (2013).

Equation 2 has been used to convert the TBS creep extension to the equivalent uniaxial creep strain, in which Δ^c is the creep extension of TBS, ε^c is the equivalent uniaxial creep strain, β is the reference stress parameter and L_0 (as shown in Figure 1) is the length between the centre of the loading pins. Similarly to η , the value of β, which is 1.4557, for the particular geometry applied in this study can be

found in the study made by Hyde et al (2013). Once these conversions have been carried out, the TBS creep curves can be compared with corresponding uniaxial curves.

$$\varepsilon^c = \frac{\Delta^c}{\beta L_0}$$

Equation 2 (Ali et al., 2015)

The preparation strategy for the specimens is showed in Figure 2. The raw LPBF built blocks (Figure 2 (a)) were fabricated on a Renishaw AM250 using Renishaw standard Inconel 718 powder (ASTM standard composition powder), with the building parameters listed in Table 1. The size distribution of the Inconel 718 powder (as shown in Figure 3) is between 15 and 45μm, the main elemental distribution are listed in Table 2. The building direction is marked by the arrow in Figure 2(a). To achieve a higher quality surface finish, the raw blocks were built with 1mm excess material. Figure 2(b) shows a specimen which is ready for testing.
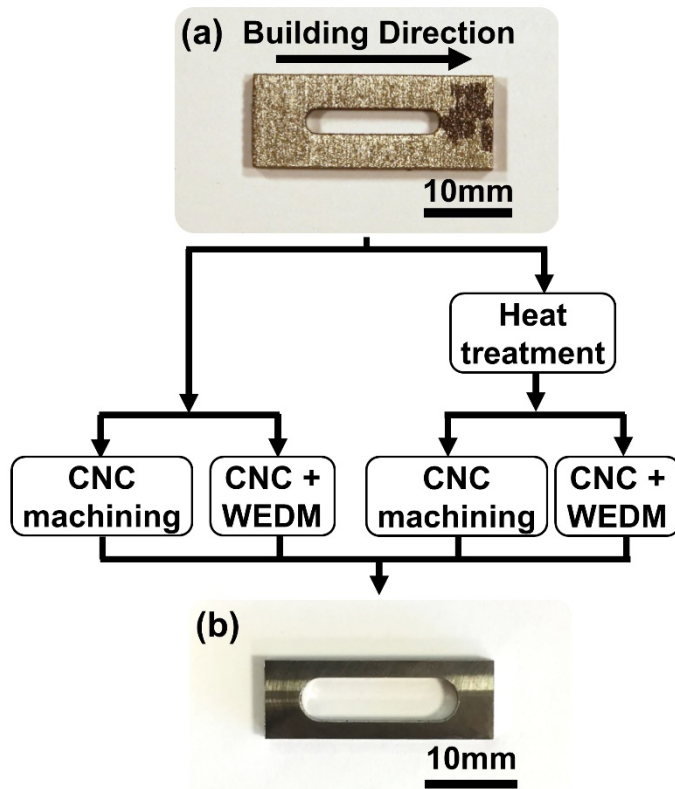
Figure 2 Diagram showing the steps taken in sample preparation, arrow in Figure 2(a) indicates the building direction

Table 1 The building parameters for raw LPBF built blocks

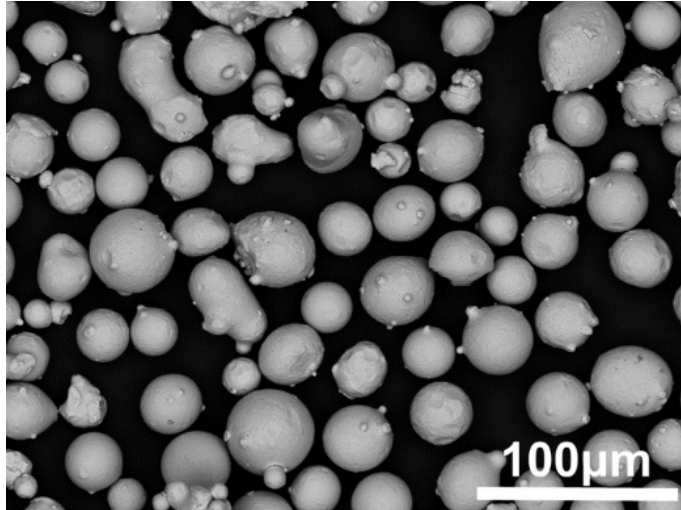| Item	Laser power / W	Point distance / μm	Exposure time / μs	Hatch distance / μm
Main body	200	70	70	100
Border	180	65	110	

Figure 3 SEM image of the Inconel 718 powder

Table 2 Chemical composition of main elements in the Inconel 718 powder

Element	Ni	Cr	Fe	Nb	Mo	Ti	Co	Al	Mg	Si
Chemical composition (wt%)	50.00 – 55.00	17.00 – 21.00	Balance	4.75 - 5.5	2.80 - 3.30	0.65 - 1.15	⩽ 1.00	0.20 - 0.80	⩽ 0.35	⩽ 0.35

To improve the material properties, 4 specimens were heat-treated according to the heat treatment strategy showed in Table 3. The purpose of the heat treatment was to increase grain size, dissolve detrimental phases (such as Laves phases) and to form strengthening precipitates (such as δ phase) at the grain boundaries. Small cubes were fabricated along with the blocks showed in Figure 2(a) to study the microstructures in both the as-build and the heat-treated conditions. They were also used to determine the surface roughness of the CNC milling and WEDM machined surfaces.

Table 3 Heat treatment strategy

Homogenization	Heat to 954 to 982 ˚C, hold for >1h, air cool or faster

Solution	Heat to 1093 ˚C ±14, hold for 1 to 2h, air cool or faster
Ageing	Heat to 718 ˚C±8, hold for 8h, air cool or faster

The effect of surface integrity on the creep performance was also considered. For most of the specimens (4 as-build and 3 heat-treated specimens), Computer Numerical Control (CNC) milling was applied (end milling for the two large surfaces and side milling for the slot and side surfaces). The surface roughness was measured with a Bruker Contour GT. For each type of surface, two measurements were made on two different samples separately. The surface roughness (R_a) of the as-build specimens were improved from around 20µm down to around 3µm after CNC milling. Another 2 specimens' (one as-build and one heat-treated) slot area was finished using Wire Electrical Discharge Machining (WEDM) technique while flat areas were machined using CNC milling. The surface roughness was reduced from around 20µm to around 6.5µm after WEDM in the slot area. Because of various heat treatments and machining processes used the specimens were divided into four different categories (as shown in Table 4). Cracks development on the CNC machined surface and the WEDM machined surface was compared after creep testing. The effect of surface integrity on lifetime and creep mechanism was also studied.

Table 4 Defined categories of the produced specimens

Specimen No.	Preparation
ABCNC 1	
ABCNC 2	In as-build condition, CNC machined.
ABCNC 3	
ABCNC 4	
ABMix	In as-build condition, CNC + WEDM machined.
HTCNC 1	
HTCNC 2	In heat-treated condition, CNC machined.
HTCNC 3	
HTMix	In heat-treated condition, CNC + WEDM machined.

The experimental parameters used in this study were in accordance with research work carried by Sugahara et al. (2012). In this work, the creep testing was carried at 650˚C with a constant stress of 750 MPa on the standard Inconel 718 uniaxial specimens. From Equation 1, the parameters applied

in this TBS creep testing are 650˚C and 747.45 MPa. The Inconel 718 samples used in Sugahara et al.'s (2012) study were melted and remelted using VIM and VAR techniques respectively for homogenization. *And the samples also went through hot forging in open die for roughing, roughing hot rolling and hot rolling finish (Sugahara et al., 2012).* For which a lifetime of 143 hours was reported.

Microstructural analysis of creep samples was undertaken before and after creep testing. Electrolytic etching solution of 10g oxalic acid in 100ml distilled water using a voltage of 6V for 8s was used to reveal the microstructure of polished specimens (Petzow, 1999). A Nikon ECLIPSE LV100ND Optical Microscope (OM), Hitachi TM3030 Scanning Electron Microscope (SEM) and JEOL 6490LV SEM which was equipped with EDS were used to observe the microstructure and chemical compositions. The fracture surfaces of the four categories of specimens (shown in Table 4) were inspected by SEM to define the fracture mechanism. An ultrasonic cleaning step was introduced to clean the fracture surfaces before to SEM inspection. The sections (showed in Figure 4) near the fracture surfaces were also analysed in the as-build and heat-treated condition using a JEOL 6490LV SEM to discern how defects develop during creep testing. The surface generated by CNC milling and WEDM were also investigated by SEM. The effects of different machining processes (CNC and WEDM) on the surface integrity of tested samples were also studied.
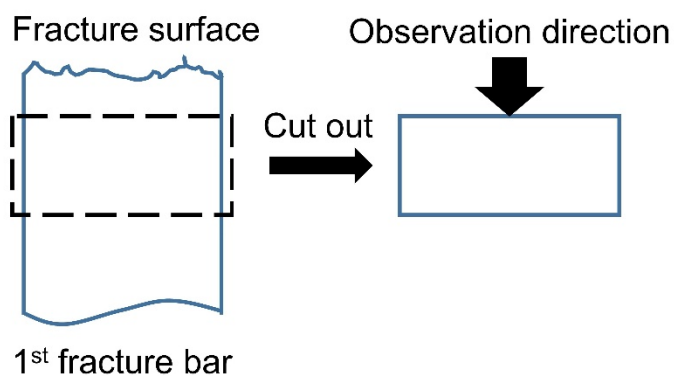
Figure 4 Diagram showing the method by which sections near fracture surface were prepared

3. Experiment results and analysis

3.1. Lifetime of specimens in creep testing

An example of a fractured creep specimen is showed in Figure 5. One of the bars (left bar (L) or right bar (R)) fractures first, followed by the other. In this study, the first broken bar (L or R) has been the focus since the failure of the second bar was not entirely due to creep related phenomena. The break sequence can be determined by the shape of the broken bars. The second broken bar generally dragged to one side due to the uneven distribution of the tensile force after the first bar has broken.
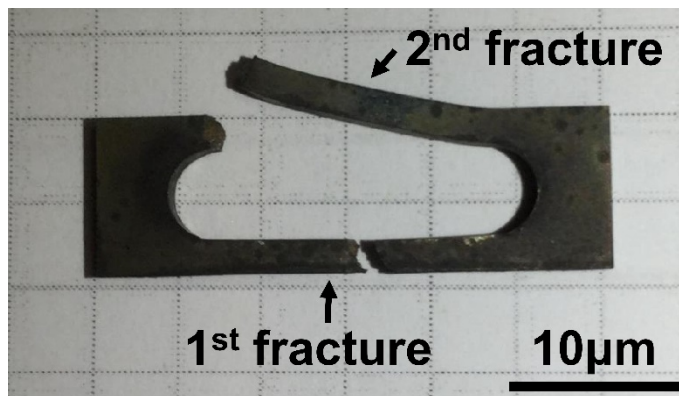

Figure 5 An example of a tested two bar specimen showing the asymmetric failure mechanism during the 2nd fracture

Figure 6 compares the lifetime between the four categories and referenced data, the data is presented in mean value plus standard error form. Regardless of the surface finish technique applied, lifetime of LPBF built samples were lower than that of wrought materials. Among the LPBF built samples the heat-treated specimen machined with CNC+WEDM techniques exhibited the longest lifetime, four times that of other samples, but still much lower compared to the reference data showed in Figure 6. The heat-treated samples machined with CNC milling have the shortest lifetime. The lifetimes of the tested specimens are also listed in Table 5.
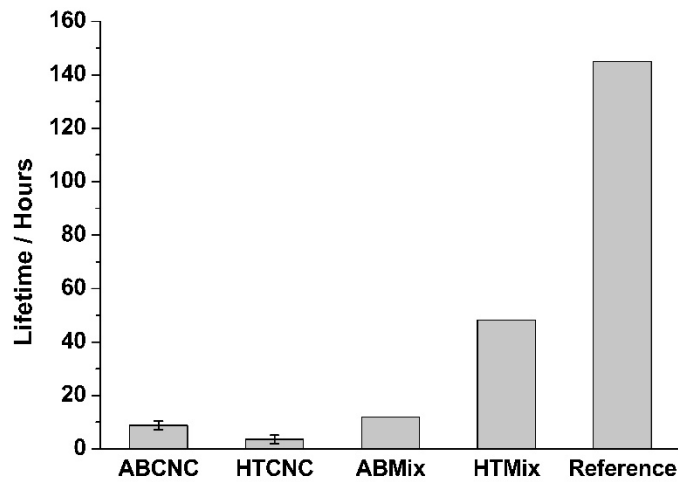
Figure 6 Comparison of the lifetime between tested TBS samples and reference data from Sugahara et al.'s (2012) study

Table 5 Lifetime of tested two bar specimens

No.	Preparation methods	Lifetime (hours)
ABCNC 1		6.73
ABCNC 2	CNC machined, in as-build condition	9.13
ABCNC 3		13.27
ABCNC 4		6.10
ABMix	CNC + WEDM machined, in as-build condition	12.00
HTCNC 1		6.40
HTCNC 2	CNC machined, in heat-treated condition	1.07
HTCNC 3		3.17
HTMix	CNC + WEDM machined, in heat-treated condition	48.27

The creep curves and minimum creep rates of tested specimens are showed in Figure 7 - Figure 9. ABCNC 1, 2, 3 and 4, as showed in Figure 7, were prepared in the same way but creep performance varied between samples. Likewise, the creep behaviour of the heat-treated specimens was also scattered as shown in Figure 8. The average minimum creep rates of both as-build and heat-treated specimens, machined with CNC only, fluctuated significantly as shown in Figure 9, and the latter is more severe.
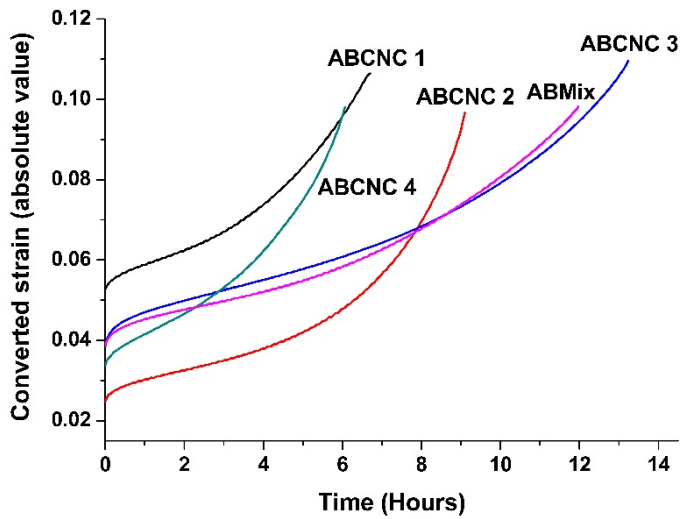
Figure 7 Creep curves of the as-build specimens, in which ABCNC 1, 2, 3 and 4 were CNC machined, and ABMix was machined with CNC+WEDM
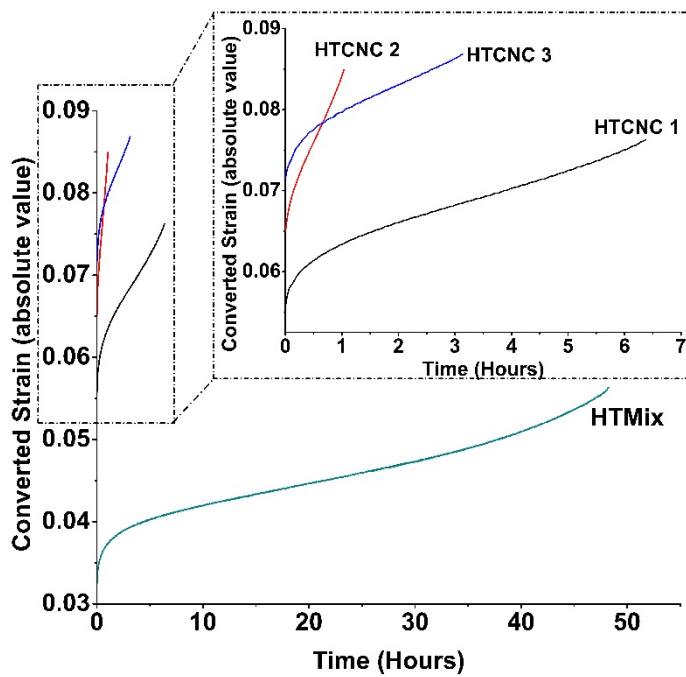
Figure 8 Creep curves of the heat-treated specimens, in which HTCNC 1, 2 and 3 were CNC machined, and HTMix was machined with CNC+WEDM. Inset provides scale for short life creep test results.
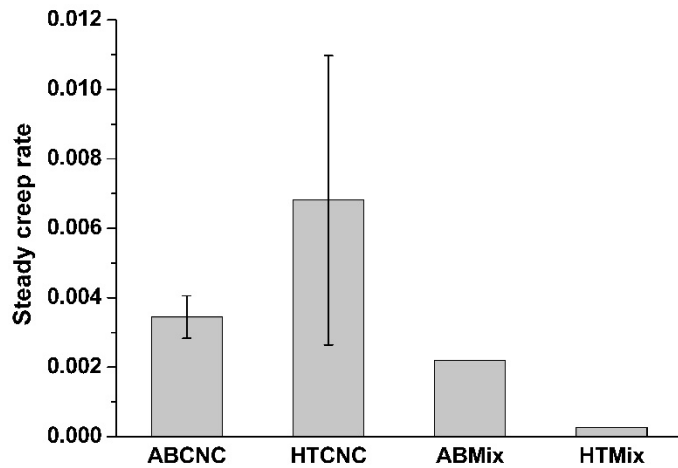
Figure 9 The comparison of the average minimum creep rates between the four categories

The comparison of creep curves between HTMix and the reference is showed in Figure 10. It is clearly showed that heat treated AM fabricated structures have poor creep performance when compared to wrought samples and a high degree of ductility. However, AM materials have the potential to gain a longer lifetime and smaller minimum creep rate with appropriate post-treatment, e.g. heat treatment.
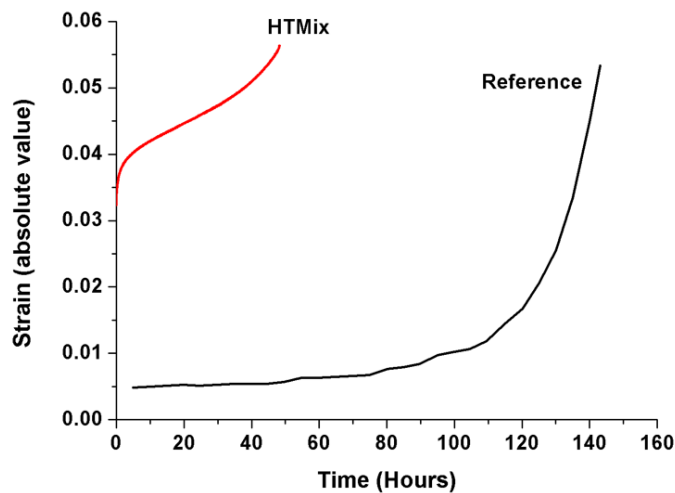
Figure 10 Comparison between the performance of HTMix and a wrought equivalent reference material (Sugahara et al., 2012)

3.2. Microstructural Analysis

The microstructure of as-build and heat-treated specimens in three mutually perpendicular planes has been analysed (as shown in Figure 11). The as-build material possesses typical microstructures observed in LPBF built structures (Chlebus et al., 2015). Laser tracks and the profile of the molten pool can be seen in three mutually perpendicular planes (as shown in Figure 11(a)). The build direction of the specimens was in the Z axis. In the heat-treated specimen, the grain sizes are much larger than the as-build equivalent. But there are no obvious marks showing the laser scanning trace and the shape of the molten pool. The microstructure is equiaxed in all three planes.
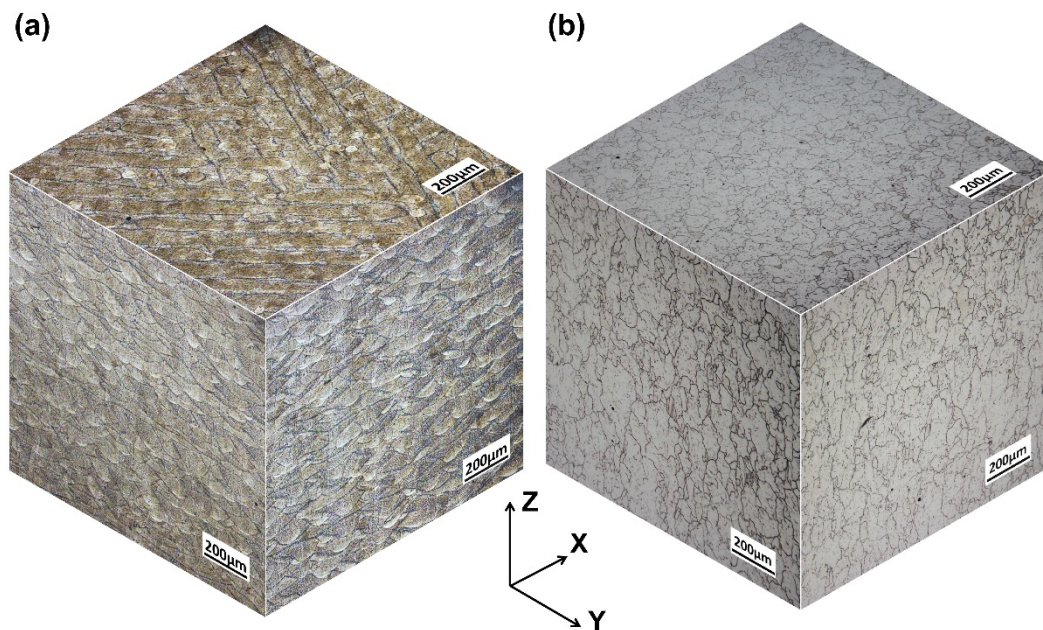
Figure 11 Microstructure of (a) as-build specimen and (b) heat-treated specimen in three mutually perpendicular planes, Z-axis is parallel to the building direction

High magnification SEM images in Figure 12 indicate the cubic sample in as-build condition (see Figure 12(a)) has a finer microstructure than the heat-treated equivalent. The heat-treated specimen possess larger grain sizes and precipitates as shown in Figure 12(b).
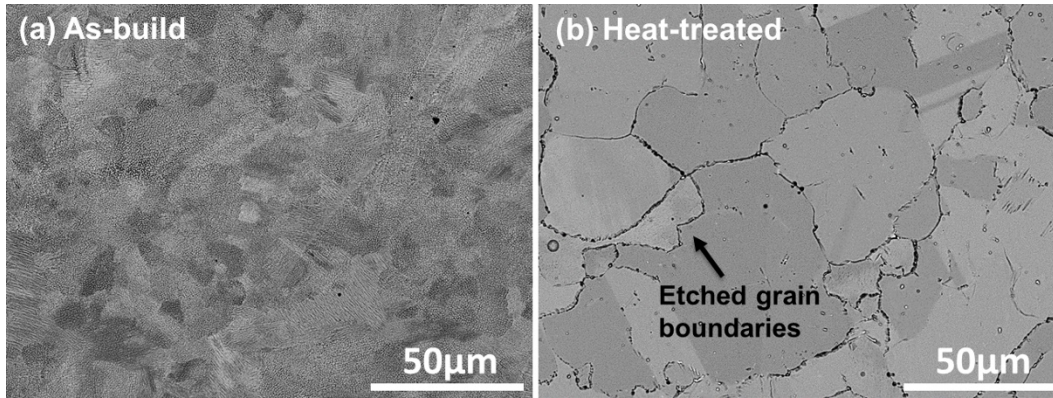
Figure 12 SEM photos of cubic samples microstructures in (a) as-build and (b) heat-treated conditions in XY plane

Energy-dispersive X-ray spectroscopy (EDS) was applied to investigate the elemental composition of these particles as shown in Figure 13. Precipitates can be observed to be spread both on grain boundaries and within the grains. For each spectrum, two measurements were made, and the average was given in Figure 13. Spectrum 1 indicates the matrix. Particles indicated by spectrum 2 have a needle shape which is typical of the δ phase (Ni_3Nb) in Inconel 718. The high volume of Nb within these particles further suggests it is δ phase. Parimi et al. (2014) also indicate that the square or spherical particles (showed by spectrum 3 & 4) which is rich in Ti and Nb is a carbide (NbC). Spectrum 5, is rich in Mo, Nb, and Ti, typical alloying elements of Laves phase. Spectrum 5 indicates Laves phase which was not fully dissolved during heat treatment.

Spectrum No. / Elemental composition wt%	1	2	3	4	5
	Matrix	δ phase	Carbide	Carbide	Laves Phase
Al	0.69	0.37	0.21	0.65	0.29
Si	0.24	0.10	0.05	0.20	0.03
Ti	0.89	1.59	6.66	1.64	8.60
Cr	19.08	9.67	8.40	18.03	10.66
Fe	18.68	8.93	7.08	17.05	10.15
Ni	50.81	54.48	17.48	49.68	25.55
Nb	5.58	22.37	57.44	9.64	35.20
Mo	4.04	2.50	2.68	3.12	9.55
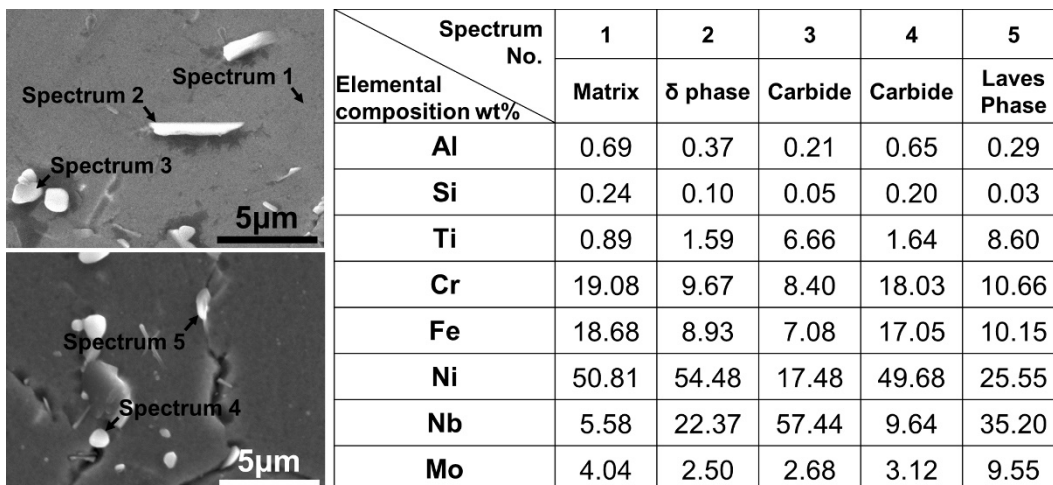
Figure 13 SEM photo of a heat-treated cubic sample showing several precipitates and their elemental compositions

3.3. Surface integrity

Since surface integrity plays an important role in the subsequent test behaviour of creep specimens. A number of preparation techniques were attempted. Figure 14 shows the surface conditions processed by CNC end milling, CNC side milling, and WEDM cutting. Key observations include; i) In CNC machined samples the near surface is characterised by localised deformation resulting from sheer through tool engagement at the surface and ii) A recast layer appeared in WEDM machined samples.
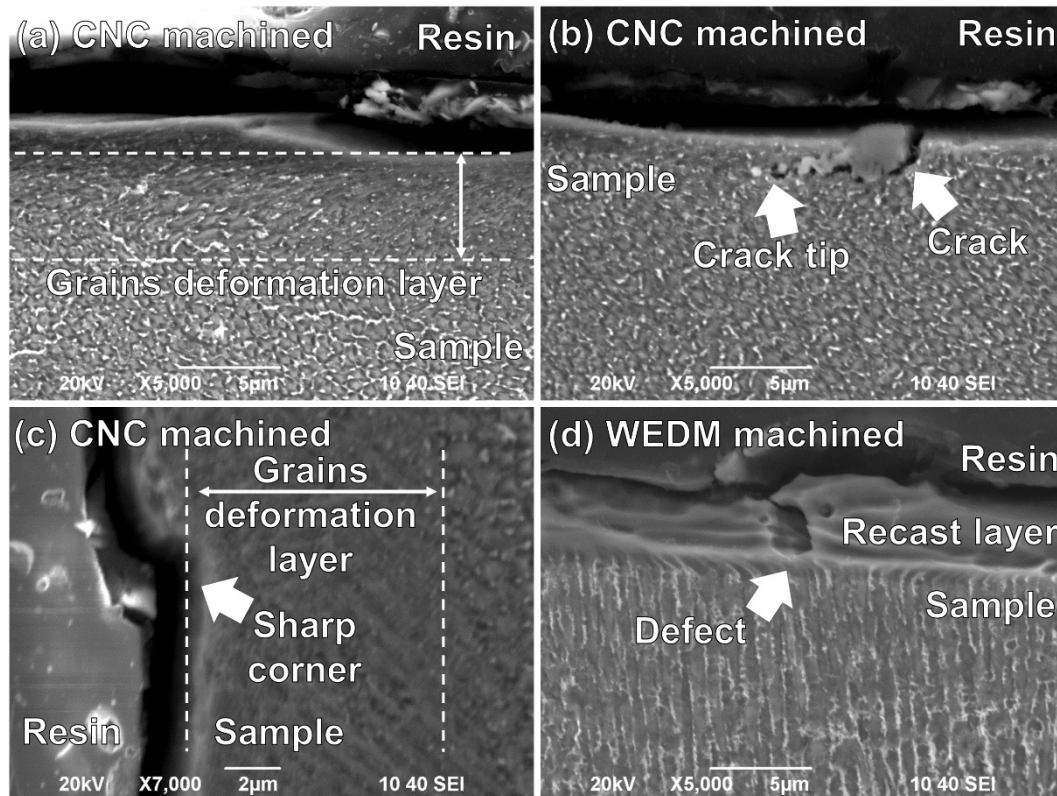

Figure 14 SEM photos of (a) deformed layer and (b) surface crack caused by CNC end milling, (c) deformed layer and defect generated in CNC side milling, and (d) recast layer in Wire EDM cutting.

Obvious deformation layers (thickness of around 10μm) can be seen in Figure 14(a) & (c). These were formed because of localised shear in the CNC milling processes and will have led to residual stresses within the material. Cracking was also observed in CNC end milled surfaces (as shown in Figure 14(b)) which appeared after the material had been lifted by the cutting blade. Crack tips were found to penetrate into the deformed layer, and such cracks are likely to penetrate further during creep testing. Sharp corners, which normally perform as stress concentration points, were found on

16

the CNC side milled surface. A recast layer was found on the WEDM cut surface as shown in Figure 14(d).

3.4. *Effects of surface integrity on surface crack development*

Cracks are observed on the surfaces machined with CNC milling in both as-build and heat-treated samples. Examples are showed in Figure 15(a) and (c) of white layers with uniform thickness where cracks penetrated into the main body through the white layer along the grain boundary, while there are no cracks observed on the surfaces machined with WEDM in either as-build or heat-treated sample (examples are showed in Figure 15(b) & (d)). After creep testing, the white layers and recast layers becomes more obvious and thicker which likely due to oxidation during creep testing.
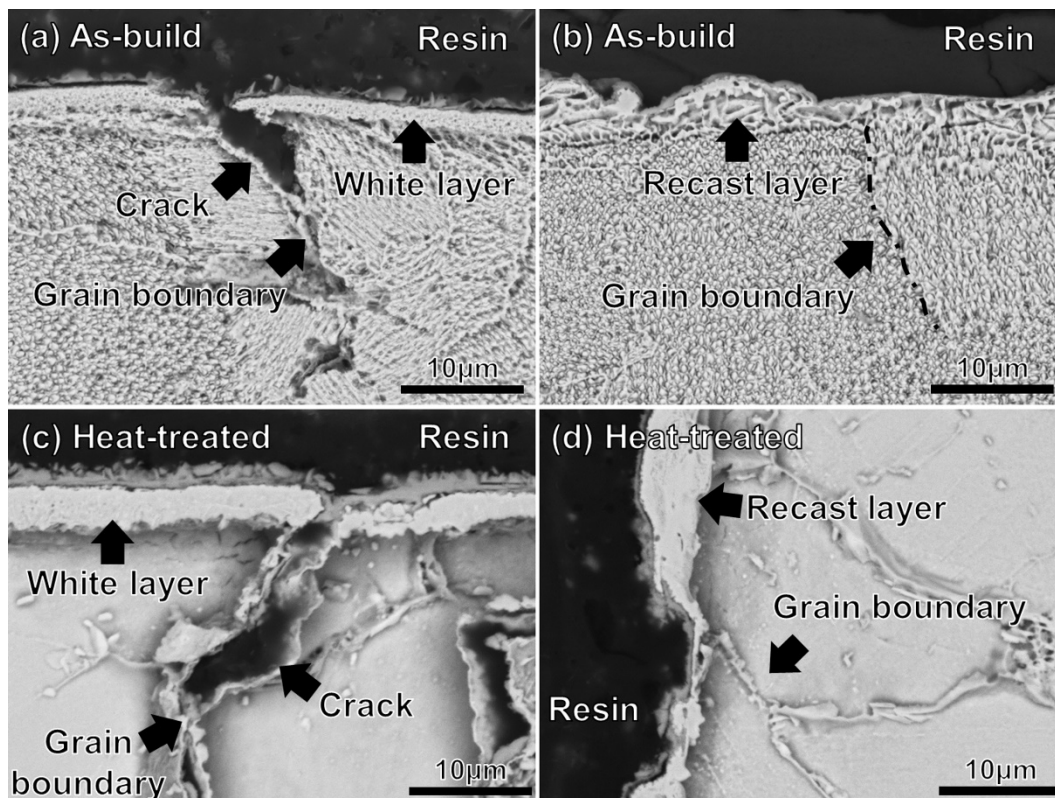
Figure 15 Conditions of surfaces treated with different methods, CNC machined (a) and WEDM cut (b) surfaces in as-build sample (ABMix), CNC machined (c) and WEDM cut (d) surfaces in heat-treated sample (HTMix)

3.5. *Fracture surfaces of tested specimens*

The fracture surfaces of all four sample types were characterised, and examples are given in Figure 16. The arrows indicate the observation directions.
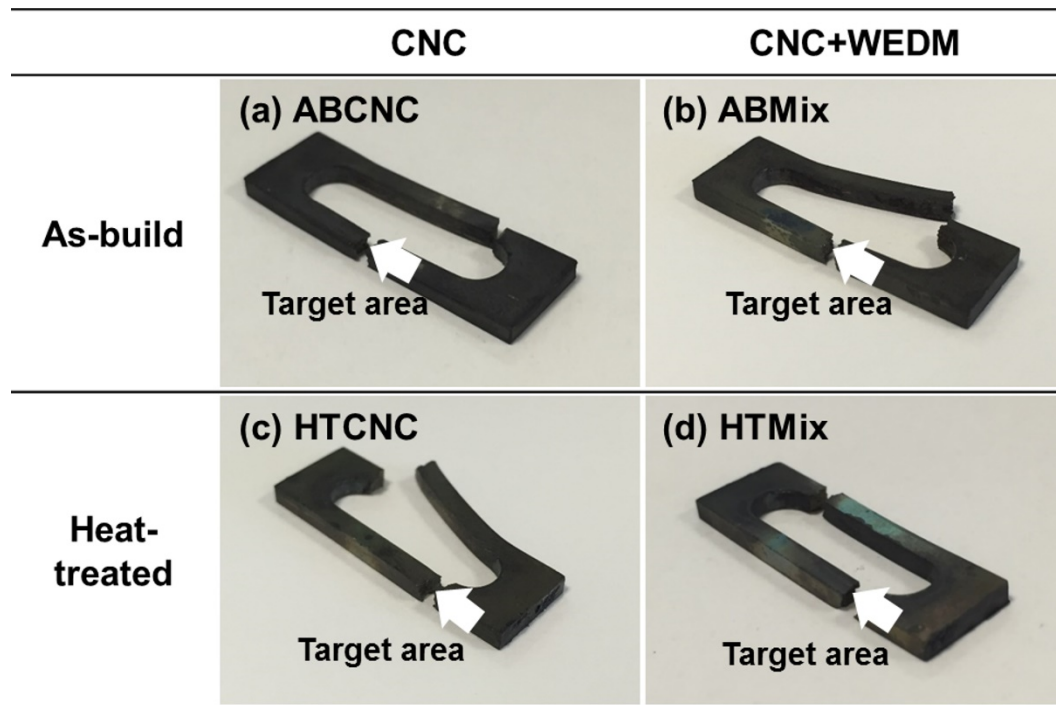
Figure 16 Failure modes in specimens selected for fracture surface analysis

An overview of the fracture surfaces is given in Figure 17. Two types of sections with different features can be seen in each fracture surface. Cracking is common in C1, C2, C3 and C4 areas, while T1, T2, T3 and T4 areas are relatively smooth but with many pores distributed throughout.
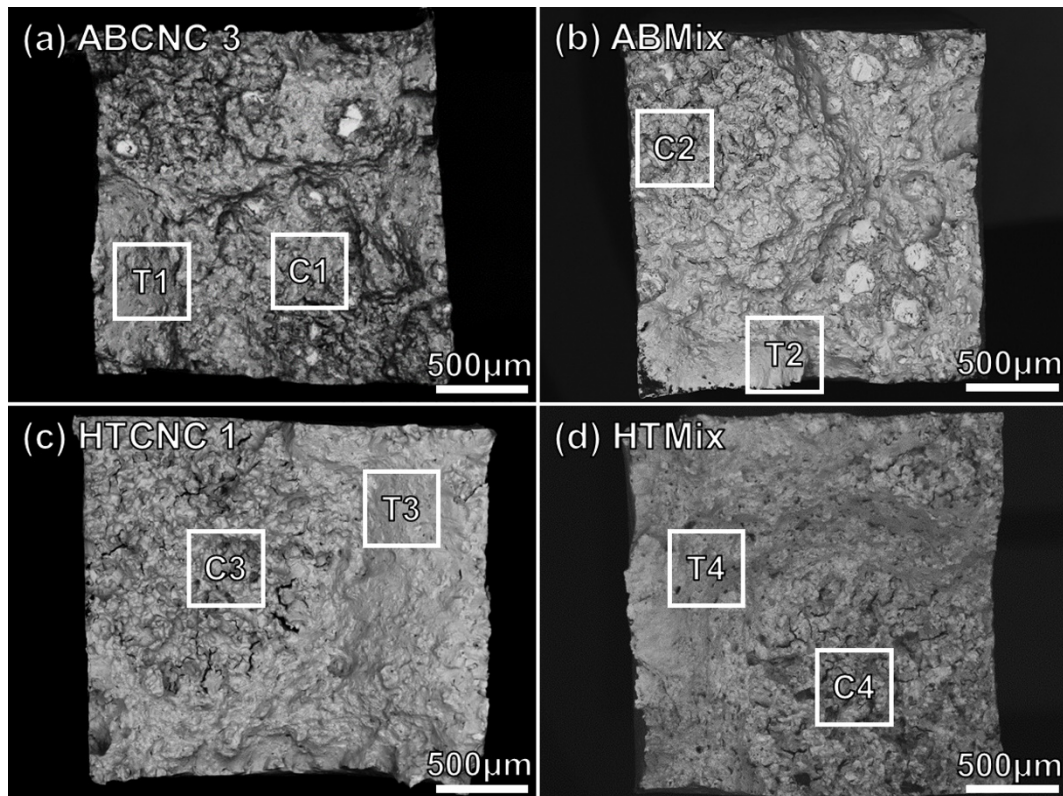
Figure 17 Overview of the fracture surfaces in ABCNC (a), ABMix (b), HTCNC (c) and HTMix (d), in which C1, C2, C3, C4 and T1, T2, T3, T4 indicate areas with marked features

Figure 18(a) shows the creep crack growth region in ABCNC. A flake shaped feature and many cracks can be seen. Tear ridges and small dimples can be seen in the higher magnification SEM image in Figure 18(b). Stripes are also observed and almost cover the whole fracture surface. They may be caused by the cleavage of dendritic structures after sufficient voids diffused to grain boundaries and large cavities formed. ABMix possesses a similar creep crack growth region as shown in Figure 18(c) and (d).

The creep crack growth region in HTCNC, as shown in Figure 18(e), has markedly different features compared to ABCNC and ABMix. The fracture surface in HTCNC is much smoother than those in the as-build samples. Cracks are observed to spread along grain boundaries. Only small tear ridges and dimples can be seen in Figure 18(e). In a high magnification SEM image (see Figure 18(f)), the fracture surface is smooth and clean but with many precipitates spread throughout. These granular precipitates may be Laves phases and carbides. The creep crack growth region in HTMix, again, shows similar features. A relatively smooth fracture surface can be seen in Figure 18(g), with many

small tear ridges and dimples. Figure 18(h) gives a clear view of these small features. Some fracture surfaces are clean with precipitates dispersed at the surface. Stripe profiles, such as the one that has been circled in Figure 18(h), are observed in HTMix. They are more likely to be slip bands in this case.
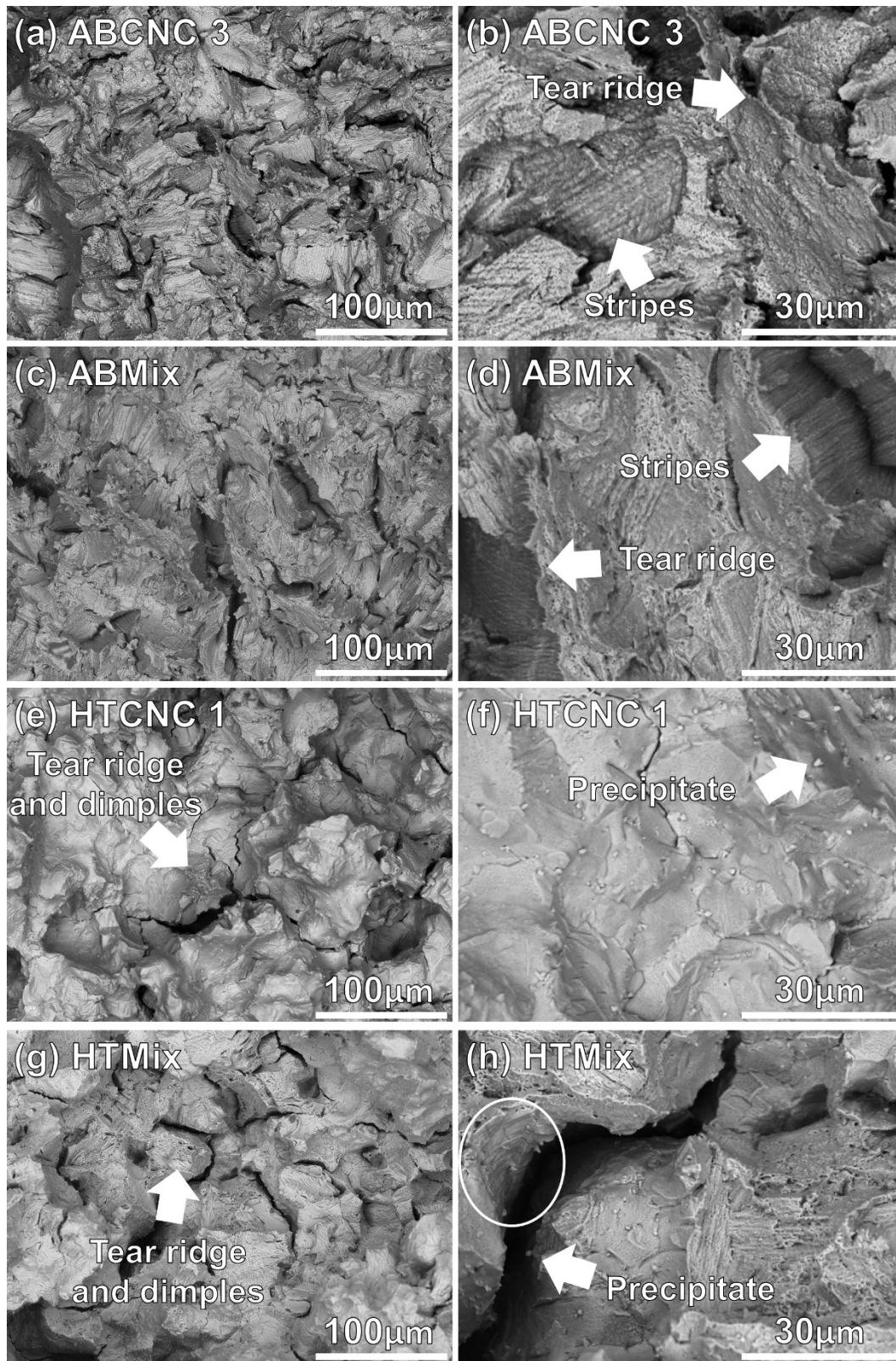
Figure 18 SEM images of the creep crack growth regions, i.e. C1 (a), C2 (c), C3 (e) and C4 (g), and the corresponding high magnification photos ((b), (d), (f) and (h)), tear ridges, dimples, stripes and precipitates are pointed out with arrows and circle

The SEM images of the mixed fracture areas in the four samples are showed in Figure 19. They are quite similar. Pores and cracks are observed (pointed out by arrows) in all of them. They are usually the starting point of material failure with cracks developing during subsequent creep testing.
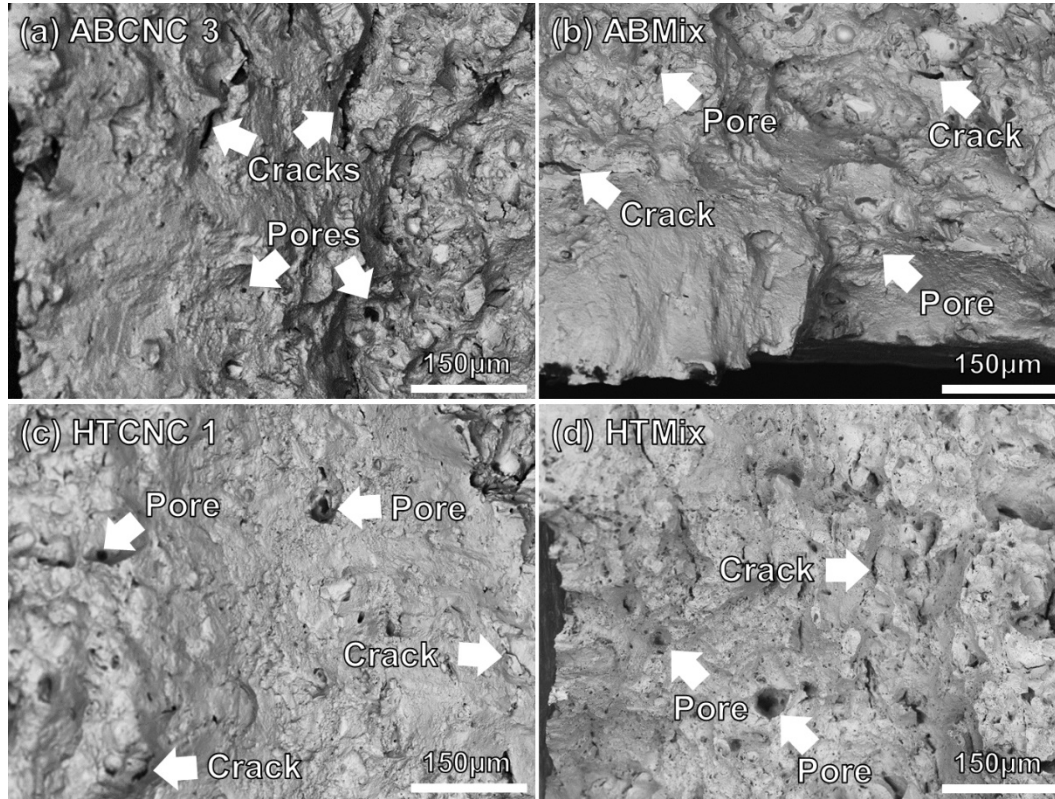
Figure 19 SEM images of the mixed fracture areas in T1 (a), T2 (b), T3 (c) and T4 (d)

3.6. Defects development in bulk materials

For the purpose of this section, samples are separated into as-build and heat-treated categories. The cross sections (obtained as shown in Figure 4) near the fracture surfaces in both samples (as shown in Figure 20) were interrogated to study the defects development during creep testing.
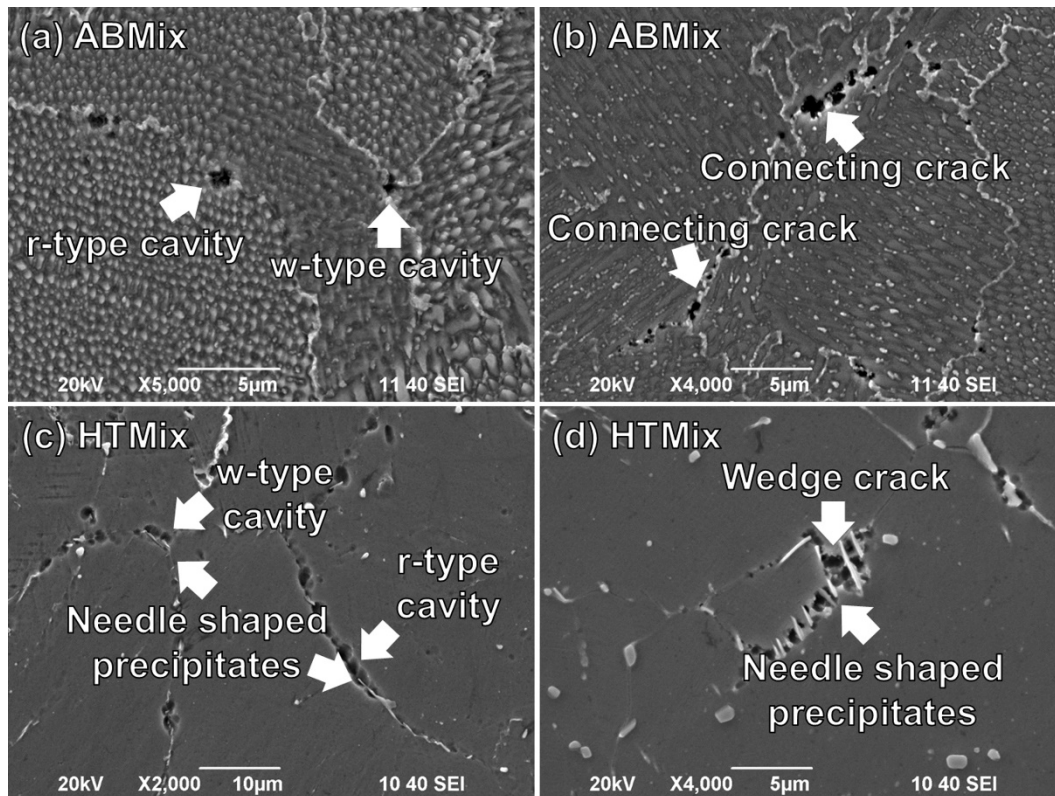
Figure 20 Sections near the fracture surfaces in as-build sample (a) & (b) and heat-treated sample (c) & (d)

In the as-build sample, both w-type (forming at the triple point of grain boundaries) and r-type (forming on the grain boundaries) cavities appeared as shown in Figure 20(a). These cavities propagated as accumulations of spherical cavities and formed large cracks along grain boundaries as shown in Figure 20(b). No pores or cracks can be seen within grains. Dendritic structures are spread all over the grains, which may give rise to the stripe profiles observed in Figure 18(b) & (d). W-type and r-type cavities are also observed in the heat-treated sample as shown in Figure 20(c). In heat-treated samples, it is found that the cavities are likely to be hindered by the needle-shaped precipitates (δ-phases) spread on the grain boundaries. In Figure 20(c), the growth of both w-type and r-type cavities are stopped by the δ-phases as shown in the figure. Figure 20(d) shows a large wedge crack generated at a triple joint between grains and its growth was obviously hindered by the δ-phases.

4. Discussion

4.1. Creep behaviour

Based on the results obtained, the creep performance of tested specimens is dictated by both the properties of the bulk material and the surface integrity. In general, the heat-treated samples which were machined with CNC+WEDM possess the best creep performance.

The lifetime of as-build specimens varies for several reasons. The appearance of the defects in the LPBF produced samples are random which serves to increase the variation. This is likely to be due to the instability, such as spatter in the build process. According to Gong et al. (2014), there are many factors related to either the building process or the LPBF system which can lead to the random generation of defects, such as pores, in the structures. In addition, the two bar specimen is sensitive to the inbuilt defects since its dimensions are much smaller than the standard uniaxial creep testing specimen. Machining defects as shown in Figure 14 will perform as the failure initiation points. However, the effects of the machining processes on the lifetimes of the as-build samples, in this case, are inconspicuous since the CNC and the CNC+WEDM machined samples have similar lifetimes. The cracks developed during creep testing showed in Figure 15(a) & (c) also serve to curtail samples lifetime.

The heat treatment was observed, as expected, to cause the growth of grain size and the precipitation of strengthening phases (δ phases and carbides) on grain boundaries, and then extend specimen lifetime. While heat-treated specimens machined with CNC milling have the shortest lifetime, in this case, large fluctuations are apparent. This may be caused by the CNC machining generating defects at the specimen surface since heat treatment made the material tougher and more difficult to be machined compared to the as-build specimens. That is to say the material response to machining will be quite different. The distributions of creep curves and minimum creep rate showed no regular pattern which indicates instability in the LPBF process. The reliability of the creep performance (as shown in Figure 7 & Figure 8) of the LPBF built specimens are poor, but the results also indicated the possibility of improving creep resistance significantly. The specimens processed subject to heat-treatment and modified machining methods displayed a lifetime four times higher than other LPBF manufactured samples.

Student's t-test was applied to statistically evaluate the lifetime data and steady creep data. For the lifetime data of ABCNC and HTCNC, p value is 0.0725, while for the steady creep rate data of

ABCNC and HTCNC, p value is 0.3881. By conventional criteria, these differences are considered to be not statistically significant. Though the mean lifetime and steady creep rate of HTCNC samples are worse compare to the ABCNC samples (as shown in Figure 6 & Figure 9), further studies are needed to confirm these differences.

4.2. Effects of heat treatment

A large number of grain boundaries in the fine microstructures (as shown in Figure 12(a)) can provide rapid diffusion paths. Diffusion along grain boundaries will lead to grain boundary sheer and cavity accumulation, thus causing severely accelerated creep (Ashby and Jones, 2012). As-build LPBF samples have an inherent weakness in their creep performance. The microstructure is the main cause for poor creep resistance. Larger grain sizes were obtained in heat-treated samples. Longer grain boundaries can slow down the cavity accumulation rate, thus improving the creep resistance. Chlebus et al. (2015) found significant secondary phases in LPBF produced Inconel 718 specimens. Laves phases are one of the common secondary phases, which can embrittle at grain boundaries and has detrimental effects on creep performance. Similar results were also observed in the studies made by Parimi et al. (2014) and Qi et al. (2009). In their studies, Laves phase was fully dissolved after solution heat treatment. However, Laves phase was apparent here and served lower the creep resistance of heat-treated samples (as shown in Figure 13). These can form the origins of pores and cracks developed during creep testing and lead to an intergranular fracture. δ phases (as shown in Figure 13) are also precipitated at the grain boundaries which can hinder crack growth according to Parimi et al. (2014), and as such improve creep performance. In general, heat-treatments need to be well controlled in order to improve creep resistance. As detailed by Radhakrishna and Prasad Rao (1997), the dissolution temperature of Laves phase in heat treatment has increased to about 1100˚C compared to the conventional at 980 ˚C. However, δ phases can also be dissolved at approximately this temperature, since its solvus temperature is around 1000˚C.

4.3. Effects of surface integrity on the creep performance

Specimens machined with CNC+WEDM displayed a much better lifetime than those machined with CNC only in both as-build and heat-treated sample groups (as shown in Figure 6). This is because machining processes can have a significant effect on the subsequent surface integrity.

Cracks started from the milled surfaces and then penetrated into the bulk materials along grain boundaries, and the white layers cannot stop the cracks growing (as shown in Figure 15(a) and (c)). WEDM generated thick recast layers (as shown in Figure 15(b) & (d)). Localised defects and material inhomogeneity appeared in the recast layer as a result of EDM, but no obvious evidence shows that the defects have penetrated into the bulk along grain boundaries. The recast layer generated is much softer than the bulk (Newton et al., 2009). Also, the grain size in the recast layer is smaller than in the main body. The material properties between the recast layer and sample's main body are so different that the interface between the two sections may be able to prevent cracks in the recast layer from penetrating into the main body. However, according to Griffiths (2001), the recast layer has detrimental effects on materials' creep performance, since it is brittle, unstable and contains cracks. Both CNC and WEDM produced unfavourable features in the machining processes. While according to the tested surfaces characterisation (see Figure 15) and creep testing results (see Figure 7 -Figure 9), WEDM is more suitable for the machining of creep testing specimens. It is proposed that further enhancements to the EDM process would significantly improve the surface integrity of components.

Another significant difference between CNC milling and WEDM lies in the presence of residual stress in the processed surfaces. According to the comparison made by Antar et al. (2012), CNC milling and WEDM generate different stress conditions on the machined surfaces. In the milled surfaces, CNC machining deformed surface grains and introduced defects and compressive residual stress to the surface layer. According to Ulutan and Ozel (2011), the residual stresses generated in the subsurface during machining processes tends to become more tensile with increasing cutting speed, feed rate, and depth of cut. While when the residual stress becomes tensile, it will enhance crack initiation and development on the machined surface. While in WEDM cut surfaces, the residual stresses are mostly tension.

4.4. Fracture mechanisms and defects development

The mechanism of the formation of two different fracture areas (as showed in Figure 17) during creep testing is illustrated in Figure 21. Voids and pores start to emerge and develop during the degradation of the whole area mainly due to creep. With the growth of the pores, they tend to connect and form large pores. While the surface defects also caused the appearance of the cracks. Pores and cracks lead to the fracture of the cross section. With the decreasing of the stressed area, the stress will exceed the yield strength and ultimate tensile strength and finally generate a mixed fracture area. Normally the regular, smooth areas appeared on the fracture surface are the interior of the pores.
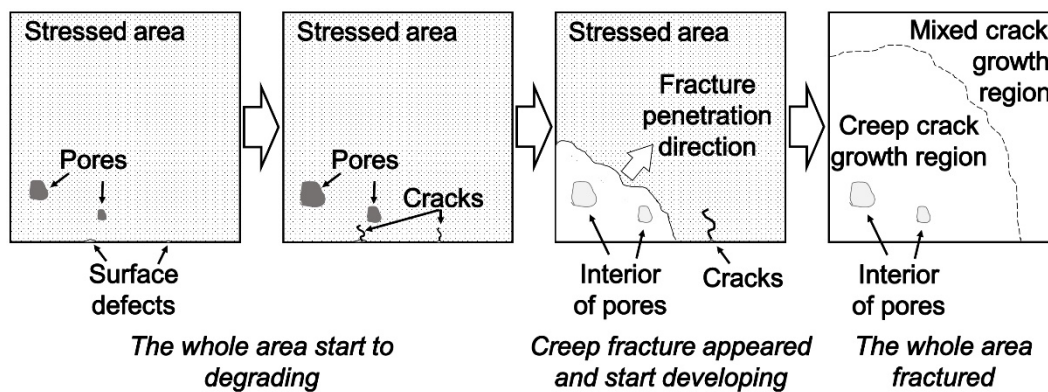
Figure 21 Schematic diagram illustrates the development of fractures during creep testing

Creep crack growth regions were similar in ABCNC and ABMix samples. The fracture features observed in Figure 18(a) & (c) indicate the creep crack growth mechanism is consistent with quasi-cleavage. While the fracture mechanisms in HTCNC and HTMix are slightly different as described in the results section as shown in Figure 18(e) & (g), although they are different only in machining processes. Intergranular fracture is dominant in the HTCNC samples. The failure mechanism of creep crack growth region in HTMix is a mixture of intergranular and quasi-cleavage fracture. In general, the features at fracture surfaces have little relationship with the surface preparation method. They are more dependent on the post-treatment technique. The properties of the bulk materials play the most important role in the formation of the fracture features.

The precipitates appear to be associated with the formation of the cavities on grain boundaries, which can serve as the cavity nucleation sites during grain boundary sliding which occurs during creep testing. In both the as-build samples and the heat-treated samples, longer cracks formed mainly due

to the accumulations of small cavities on grain boundaries (as shown in Figure 20(b) & (c)). In the as-build samples, grain boundary sliding is likely to happen and cause the nucleation of cavities due to the small grain size and less effective strengthening precipitates. While in heat-treated samples, large grain size and beneficial strengthening precipitates (as showed in Figure 20(d)) are consistent with a better creep resistance.

Conclusions

Inconel 718 specimens built by LPBF have relatively poor creep resistance. Both as-build and heat-treated specimens have much shorter lifetime and higher minimum creep rate compared to the results obtained by Sugahara et al. (2012) with wrought specimens. This presents a fundamental limitation to designers seeking to exploit LPBF for high-value applications.

W-type and r-type cavities appeared in both as-build and heat-treated samples, cracks formed mainly due to the accumulations of small cavities at grain boundaries. In heat-treated samples, δ-phase showed a strong function of stopping crack growth.

Surface integrity does have influences on the creep performance of LPBF made Inconel 718 samples. The primary mechanisms are likely to be surface finish and residual stresses. WEDM machined samples showed better creep resistance than CNC machined samples in this study.

Both machining processes applied in this study generated unfavourable structures and changed the surface integrity of the samples. The effects of residual stresses generated during machining on creep performance are something of interest and worthy of further exploration.

A better way to achieve the full control of the surface integrity before creep testing with TBS is required. Mechanical polishing and electropolishing are potential options to eliminate the effects of surface integrity that are caused by machining processes.

At the present stage, post-treatment, such as heat treatment, is still necessary for obtaining good creep performance in LPBF manufactured specimens.

This study provides a fundamental first study into the creep performance of LPBF built Inconel 718 samples with TBS and form the basis of an entirely new research agenda to improve L component creep resistance.

Acknowledgements

References

Ali, B.S.M., Hyde, T.H., Sun, W., 2015. Small Two-Bar Specimen Creep Testing of Grade P91 Steel at 650°C. High Temperature Materials and Processes, 35, pp. 243-252.

Amato, K.N., Gaytan, S.M., Murr, L.E., Martinez, E., Shindo, P.W., Hernandez, J., Collins, S., Medina, F., 2012. Microstructures and mechanical behavior of Inconel 718 fabricated by selective laser melting. Acta Materialia, 60, pp. 2229-2239.

Antar, M.T., Soo, S.L., Aspinwall, D.K., Sage, C., Cuttell, M., Perez, R., Winn, A.J., 2012. Fatigue response of Udimet 720 following minimum damage wire electrical discharge machining. Materials & Design, 42, pp. 295-300.

Ashby, M.F., Jones, D.R.H., 2012. Engineering Materials 1 - An Introduction to Properties, Applications, and Design, fourth ed. Elsevier, pp. 337-345.

Chlebus, E., Gruber, K., Kuźnicka, B., Kurzac, J., Kurzynowski, T., 2015. Effect of heat treatment on the microstructure and mechanical properties of Inconel 718 processed by selective laser melting. Materials Science and Engineering: A, 639, pp. 647-655.

Diboine, A., Pineau, A., 1987. Creep crack initiation and growth in Inconel 718 alloy at 650°C. Fatigue & Fracture of Engineering Materials & Structures, 10, pp. 141-151.

Diltemiz, S.F., Zhang, S., 2013. Superalloys for super jobs, In: Zhang, S., Zhao, D. (Eds.), Aerospace Material Handbook. CRC Press, London, pp. 1-76.

Gibson, I., Rosen, D.W., Stucker, B., 2010. Additive Manufacturing Technologies: Rapid Prototyping to Direct Digital Manufacturing. Springer, New York, pp. 103-142.

Gong, H., Rafi, K., Gu, H., Starr, T., Stucker, B., 2014. Analysis of defect generation in Ti–6Al–4V parts made using powder bed fusion additive manufacturing processes. Additive Manufacturing, 1–4, pp. 87-98.

Griffiths, B., 2001. Manufacturing Surface Technology: Surface Integrity & Functional Performance. Penton Press, London, pp. 176-177.

Hann, B.A., 2016. Powder Reuse and Its Effects on Laser Based Powder Fusion Additive Manufactured Alloy 718. SAE Int. J. Aerosp., 9, pp. 209-213.

Hyde, T.H., Ali, B.S.M., Sun, W., 2013. Analysis and Design of a Small, Two-Bar Creep Test Specimen. Journal of Engineering Materials and Technology, 135, pp. 041006-041006.

Kassner, M.E., 2009. Fundamentals of Creep in Metals and Alloys, sceond ed. Elsevier, pp. 225-231.

Liu, C.D., Han, Y.F., Yan, M.G., Chaturvedi, M.C., 1991. Creep crack growth behavior of alloy 718. Superalloys 718, 625 and Various Derivatives, pp. 537-548.

Liu, F., Lin, X., Yang, G., Song, M., Chen, J., Huang, W., 2011. Microstructure and residual stress of laser rapid formed Inconel 718 nickel-base superalloy. Optics & Laser Technology, 43, pp. 208-213.

Lu, Y., Wu, S., Gan, Y., Huang, T., Yang, C., Junjie, L., Lin, J., 2015. Study on the microstructure, mechanical property and residual stress of SLM Inconel-718 alloy manufactured by differing island scanning strategy. Optics & Laser Technology, 75, pp. 197-206.

M'Saoubi, R., Outeiro, J., Chandrasekaran, H., Dillon Jr, O., Jawahir, I., 2008. A review of surface integrity in machining and its impact on functional performance and life of machined products. International Journal of Sustainable Manufacturing, 1, pp. 203-236.

Mercelis, P., Kruth, J.P., 2006. Residual stresses in selective laser sintering and selective laser melting. Rapid Prototyping Journal, 12, pp. 254-265.

Nadammal, N., Cabeza, S., Mishurova, T., Thiede, T., Kromm, A., Seyfert, C., Farahbod, L., Haberland, C., Schneider, J.A., Portella, P.D., Bruno, G., 2017. Effect of hatch length on the development of microstructure, texture and residual stresses in selective laser melted superalloy Inconel 718. Materials & Design, 134, pp. 139-150.

Newton, T.R., Melkote, S.N., Watkins, T.R., Trejo, R.M., Reister, L., 2009. Investigation of the effect of process parameters on the formation and characteristics of recast layer in wire-EDM of Inconel 718. Materials Science and Engineering: A, 513–514, pp. 208-215.

Parimi, L.L., A, R.G., Clark, D., Attallah, M.M., 2014. Microstructural and texture development in direct laser fabricated IN718. Materials Characterization, 89, pp. 102-111.

Petzow, G., 1999. Metallographic etching : techniques for metallography, ceramography, plastography, 2nd ed. ASM International Materials Park, Ohio, pp. 125.

Prater, T., Tilson, W., Jones, Z., 2015. Characterization of Machine Variability and Progressive Heat Treatment in Selective Laser Melting of Inconel 718, JANNAF Joint Propulsion Conference, Nashville, TN; United States.

Qi, H., Azer, M., Ritter, A., 2009. Studies of Standard Heat Treatment Effects on Microstructure and Mechanical Properties of Laser Net Shape Manufactured INCONEL 718. Metall and Mat Trans A, 40, pp. 2410-2422.

Radhakrishna, C., Prasad Rao, K., 1997. The formation and control of Laves phase in superalloy 718 welds. Journal of Materials Science, 32, pp. 1977-1984.

Schafrik, R.E., Ward, D.D., Groh, J.R., 2001. Application of Alloy 718 in GE Aircraft Engines: Past, Present and Next Five Years In: Loria, E.A. (Ed.), Superalloys 718, 625, 706 and Various Derivatives TMS, Warrendale, PA, pp. 1-11.

Song, B., Zhao, X., Li, S., Han, C., Wei, Q., Wen, S., Liu, J., Shi, Y., 2015. Differences in microstructure and properties between selective laser melting and traditional manufacturing for fabrication of metal parts: A review. Frontiers of Mechanical Engineering, 10, pp. 111-125.

Sugahara, T., Martinolli, K., Reis, D.A.P., Neto, C.d.M., Couto, A.A., Neto, F.P., Barboza, M.J.R., 2012. Creep Behavior of the Inconel 718 Superalloy. Defect and Diffusion Forum, 326-328, pp. 509-514.

Tucho, W.M., Cuvillier, P., Sjolyst-Kverneland, A., Hansen, V., 2017. Microstructure and hardness studies of Inconel 718 manufactured by selective laser melting before and after solution heat treatment. Materials Science and Engineering: A, 689, pp. 220-232.

Ulutan, D., Ozel, T., 2011. Machining induced surface integrity in titanium and nickel alloys: A review. International Journal of Machine Tools and Manufacture, 51, pp. 250-280.

Wang, F., 2011. Mechanical property study on rapid additive layer manufacture Hastelloy® X alloy by selective laser melting technology. Int J Adv Manuf Technol, 58, pp. 545-551.

Wen, S., Zhou, S., Liu, X., 2016. Effect of Surface Roughness on the Determination of the Creep Properties of Material by Using Three Points Bending Creep Test, International Symposium on Mechanical Engineering and Material Science (ISMEMS 2016). Atlantis Press, pp. 22-28.

Xia, M., Gu, D., Yu, G., Dai, D., Chen, H., Shi, Q., 2016. Influence of hatch spacing on heat and mass transfer, thermodynamics and laser processability during additive manufacturing of Inconel 718 alloy. International Journal of Machine Tools and Manufacture, 109, pp. 147-157.

Yadollahi, A., Shamsaei, N., Thompson, S.M., Elwany, A., Bian, L., 2017. Effects of building orientation and heat treatment on fatigue behavior of selective laser melted 17-4 PH stainless steel. International Journal of Fatigue, 94, pp. 218-235.

Figure and table captions